Composites: Part A 166 (2023) 107380

Contents lists available at ScienceDirect

Composites Part A

journal homepage: www.elsevier.com/locate/compositesa

Developing a high-efficiency predictive model for self-temperature-compensated piezoresistive properties of carbon nanotube/graphene nanoplatelet polymer-based nanocomposites

Mojtaba Haghgoo [a], Reza Ansari [a], Sung-Hwan Jang [b,*], Mohammad Kazem Hassanzadeh-Aghdam [c,*], Mohammad Nankali [d]

[a] Faculty of Mechanical Engineering, University of Guilan, Rasht, Iran
[b] Department of Civil & Environmental Engineering, School of Engineering, Hanyang University ERICA, Ansan, Gyeonggi-do 15588, South Korea
[c] Department of Engineering Science, Faculty of Technology and Engineering, East of Guilan, University of Guilan, Rudsar-Vajargah, Iran
[d] Department of Mechanical Engineering, Iran University of Science and Technology, Tehran, Iran

ARTICLE INFO

Keywords:
A. Multifunctional composites
B. Hybrid
C. Electrical properties
D. Analytical modeling

ABSTRACT

The thermo-resistive and piezoresistive responses of carbon nanotube (CNT)/graphene nanoplatelet (GNP) polymer-based nanocomposites are analytically investigated. The 3D representative volume element is generated by the Monte Carlo approach to incorporate the random distribution of nanofillers. The Monte Carlo approach is paired with the percolation model to investigate the percolation behavior of the nanocomposite. The validity of the analytical model is verified by comparing the predicted results with the experimental data. The Poisson's ratio and height of barrier potential influence on the piezoresistivity of nanocomposite are studied. Analytical results determine the aspect ratio and influence of carbon nanotube degree of orientation on thermoresistivity of nanocomposite. The effects of intrinsic and physical properties of GNPs on resistivity change with temperature are investigated. It is found that nanocomposite filled with CNTs presented lower percolation threshold than those filled with GNPs. The results also revealed that the filler alignment caused a higher piezoresistivity.

1. Introduction

Since the primary developments in strain sensors, different types of nanofillers such as carbon nanotubes (CNTs) and graphene nanoplatelets (GNPs) have been used to add astonishing thermal, electrical and mechanical properties into the transparent electrodes and flexible electronics [1]. Manipulating several factors such as concentration and aspect ratio of nanofillers has a role in adding these attractive properties to nanocomposites [2]. These polymer nanocomposites possess high-strength and light-weight and thus provide improved overall mechanical properties [3]. The astonishing mechanical properties are attributed to ideal reinforcing properties of nanofillers [4], strong interfacial adhesion between matrix and nanofillers [5] and enhanced strength of added nanofiller along with CNTs [6] in ternary nanocomposite which is made of two types of conductive nanofillers [7]. The discovery of their electrical behavior dominated by percolation led to a wide interest of their usage to reduce the weight of the material, i.e. for health monitoring and wearable bioelectronics [8,9]. In these applications, improvement of electrical conductivity is an important task for material development with the excellent efficiency for production with the synergistic and tunable properties [10,11].

As the nanofiller volume fraction is close to a certain volume fraction (percolation threshold), the small increase of volume fraction results in the drastic change in electrical conductivity due to the formation of the first conductive pathways. Conductive pathways formed by the nanofillers lead to a percolated behavior [12,13]. The term percolated system refers to configurations with formed conductive paths where an abrupt transition occurs in electrical properties. It is well declared that the percolation threshold of nanocomposites is governed by several physical and intrinsic properties such as, length, filler alignment and intrinsic electrical conductivity [14]. CNTs extraordinary charge carrying capacity candidates them to bring low percolation threshold to the nanocomposites [15].

It is revealed that the electrical properties of strain sensors are manipulated by some foreign stimulation such as strain. This property is dedicated by piezoresistive behavior that is defined as the electrical

* Corresponding authors.
E-mail addresses: sj2527@hanyang.ac.kr (S.-H. Jang), mk.hassanzadeh@gmail.com (M. Kazem Hassanzadeh-Aghdam).

https://doi.org/10.1016/j.compositesa.2022.107380
Received 18 October 2022; Received in revised form 12 December 2022; Accepted 13 December 2022
Available online 17 December 2022

resistance change with the strain [16,17]. The exceptional improvements of mechanical properties [18], thermal stability [19] and electrical conductivity given by nanofillers make device sensitive enough to strain and also independent to temperature change [20]. These improvements have transformed the focus to self-temperature-compensated strain sensors [21]. Since, the behavior of nanocomposites depends on the properties of their components [22], significant advances in using CNTs and GNPs in strain sensors have opened a new era by using the synergistic effect of hybrid filler system for sensing multiple stimuli caused by strain and temperature simultaneously.

Researchers have developed computational models to elucidate the variation of electrical properties with respect to various parameters. Chang et al. [23] theoretically modeled the piezoresistive response in mechanically deformed composites. They investigated the prospect of nanofiller alignment by imposing controlled mechanical strain to improve electron transport efficiency. They declared enhanced electrical conductivity by forcing alignment which improved the percolated network. Cen-Puc et al. [24] investigated the mechanism governing thermoresistivity of CNT polymer composites theoretically and experimentally. They proposed two modeling approaches based on a classical tunneling model and general effective medium theory to predict the dependence of the electrical resistance with temperature. Both models predicted positive temperature coefficient of resistance (PTC) for CNT weight percent below 50%. Maffucci et al. [25] demonstrated the possibility of exhibiting a negative temperature coefficient of resistance (NTC) in larger fractions of CNTs. They used an electro-thermal model to define the conditions under which a negative change of the resistance may be observed. They showed NTC for longer CNTs at lower temperatures. Morais et al. [26] investigated the electrical conductivity of single walled carbon nanotubes (SWCNT) epoxy composite under external electric field. They investigated the effect of electric field and particle concentration on the rotation and interconnection of SWCNTs. Inter-nanotube distances between two SWCNTs were evaluated using finite element models. They declared the influence of contact points between the particles on the percolation and resistivity. Sibilia et al. [27] studied the temperature dependence of the electrical resistivity of GNP epoxy nanocomposite analytically. They reported a linear trend of resistivity in a wide temperature range −60 to 60 °C. They found that the room temperature resistivity fell with a temperature coefficient of resistance (TCR) of $-1.55.10^{-3}$ (1/°C). They determined the effect of contact resistance negligible. Tran et al. [28] investigated the input of graphene combined with CNTs to build thermoplastic polyurethane functionalized hybrid nanocomposite. They found the increase of piezoresistive response by introducing graphene in nanocomposite where GNPs kept contact with CNTs by orientating and sliding.

Researchers have fabricated stretchable nanocomposites containing carbon nanofillers with beneficial thermoresistive properties. These nano-sensors showed high temperature sensitivity and good linearity promising their use as smart coating materials for heat detection [29,30]. Lasater et al. [31] investigated the thermoresistive behavior of nanocomposites with electrically conductive networks of CNTs in a vinyl ester matrix. They studied a series of specimens above the percolation threshold 0.1 wt%. They reported that thermoresistive behavior was strongly dependent on the CNT content, thermal expansion and polymer motion. They declared that TCR varied with temperature at higher CNT content. Li et al. [32] fabricated CNT-polyimide (PI) and GNP-PI nanocomposite thin film strain sensors and characterized their electromechanically properties. They determined the percolation threshold and piezoresistivity using inkjet printing technique and uniaxial tensile tests. They declared that GNP-PI nanocomposite thin film exhibited higher strain sensitivity compared to CNT-PI nanocomposite. Liu et al. [33] proposed a systematic study to explore the PTC phenomenon and the underlying mechanism taking account of CNTs, GNPs and high density polyethylene (HDPE). They reported that excessive contact points with highly interconnected networks can result in an NTC effect. They declared that highest PTC occurred around percolation threshold with the minimum number of conductive pathways. Pech-Piste et al. [34] investigated the electromechanical, piezoresistive and thermoresistive behavior of polysulfone nanocomposites using a hybrid combination of graphene sheets (GSs) and multi-walled carbon nanotubes (MWCNTs). Their results showed the highest electrical conductivity was achieved for nanocomposites with only CNTs downplaying the role of GSs to improve the electrical conductivity. They revealed that two carbon nanostructures with different dimensionality could improve the piezoresistive and thermoresistive properties of polymer composites. Sanli et al. [35] deposited CNTs directly on a glass-reinforced epoxy beam on the same axis with strain gauge. They observed relatively higher sensitivities for 0.5 wt% CNT polymer nanocomposite than commercial strain gauges. They found that nanocomposite demonstrated NTC behavior under cyclic temperature range from 0 to 80 °C. Turkani et al. [36] developed a fully printed CNT based NTC thermistor for temperature sensing applications. The multi-layer NTC thermistor was fabricated using additive print manufacturing process on a flexible polyethylene terephthalate (PET) substrate. They reported that as the temperature was increased from −40 to 100 °C, the resistive response of the thermistor decreased exponentially. Verma et al. [37] examined the thermo-resistive and thermo-piezoresistive sensitivity of MWCNT/polypropylene nanocomposites. They reported NTC behavior for heated nanocomposites. The highest thermo-resistive sensitivity was measured for the composite with the lowest MWCNT content. They declared that increased thermo-piezoresistivity with the increase of temperature was activated by thermally assisted hopping.

Developing a hybrid sensing material with low TCR can be done by offsetting the positive and negative temperature dependences. Temperature dependence of polymer composites with conducting fillers leans on intrinsic properties of polymers and fillers, and physical distribution of the fillers in the polymer matrix. One of the significant engineering challenges is finding the effective combination of fillers to offer efficient properties. This paper aims to develop a new 3D modeling approach to predict the self-temperature compensated piezoresistive behavior of CNT/GNP polymer nanocomposites using 3D Monte-Carlo algorithm paired with percolation network model. Different parameters are considered in the model, such as the length, diameter, aspect ratio and orientation angle of CNTs and GNPs, other engaged parameters are the effects of quantum tunneling distance, volume fraction, TCR, potential barrier height and Poisson's ratio of polymer matrix. In this context, a model is first established that can disperse the CNTs and GNPs with several random locations and orientations. Then, resistivity evolution as a function of strain can be evaluated. The effects of interactions between nanotubes and nanoplatelets have been considered. It is found that in the case of lower GNP size, the tunneling effect plays a significant role in the nanocomposites.

2. Analytical percolation model

2.1. Monte-Carlo approach

The algorithm for modeling the electrical conductivity of nanocomposites includes several steps from creating random nanofiller network to finding the separation distances between nanofillers. The established simulation model considers tunneling region inside the polymer matrix to form network structures [38] and determines the electrical percolation [39]. It is assumed that the nanocomposite is made up of some repeated structures which occupy a volume small enough to help the percolation to be accurately described for the whole nanocomposite. Monte-Carlo simulation method is used to locate the center point (x_c^i, y_c^i, z_c^i) of the i th CNT, its coordinates (θ_i, ϕ_i) and length l^i in a rectangular representative volume element (RVE) with a dimension of $L_x \times L_y \times L_z$ by using a random number generated on the interval {0,1}. Eq. (1) represents the center point, azimuthal and polar angles of a randomly oriented CNTs [40].

$$\begin{bmatrix} x_c^i \\ y_c^i \\ z_c^i \\ \phi^i \\ \theta^i \end{bmatrix} = \begin{bmatrix} L_x \times \text{rand} \\ L_y \times \text{rand} \\ L_z \times \text{rand} \\ 2\pi \times \text{rand} \\ \cos^{-1}(2 \times \text{rand} - 1) \end{bmatrix} \quad (1)$$

The primary orientation state of CNTs was allocated by arbitrary azimuthal and polar angles. This provides the effect of the random geometries with different lengths on an isotropic medium. The CNT alignment is fulfilled by restricting its orientation with the in-plane Θ and out-of-plane Φ angles. CNTs' alignment imparts anisotropy to nanocomposite and influences the electrical behavior.

The starting and ending points of the i-th CNT with length l^i and diameter d^i are expressed as depicted in Eq. (2) [41].

$$\begin{Bmatrix} x_0^i \\ y_0^i \\ z_0^i \end{Bmatrix} = \begin{Bmatrix} x_c^i \\ y_c^i \\ z_c^i \end{Bmatrix} - (l^i/2) \begin{Bmatrix} \sin\theta^i \cos\phi^i \\ \sin\theta^i \sin\phi^i \\ \cos\theta^i \end{Bmatrix}$$

$$\begin{Bmatrix} x_1^i \\ y_1^i \\ z_1^i \end{Bmatrix} = \begin{Bmatrix} x_c^i \\ y_c^i \\ z_c^i \end{Bmatrix} + (l^i/2) \begin{Bmatrix} \sin\theta^i \cos\phi^i \\ \sin\theta^i \sin\phi^i \\ \cos\theta^i \end{Bmatrix} \quad (2)$$

Random generation of CNTs is repeated until the desired volume fraction is achieved. Generation proceeds with eliminating newly added overlapped CNTs separated in a distance less than the van der Waals distance ($d_{\text{vdW}} = 0.34nm$) to avoid penetration. The CNTs need to be in tunneling distance range which means two CNTs are close enough to form a conductive pathway. When the connection possibility is provided, the intersection between the CNT pair is achieved.

The nanometer distance which electrons can penetrate is deduced by cutoff distance d_{cutoff} which indicates the range in which the electron transport can happen between CNTs. A linear dependence is witnessed when CNTs are in contact with each other, which means that although CNTs possess different lengths, it is reasonable to give all CNTs the same length due to the small segment along the length of two CNTs considered connected in the model.

GNPs are impenetrable elliptical disks with a defined thickness. When in tunneling distance range, the minimum distance between their mid-surfaces is lower than the cutoff distance added to their thickness. If an elliptical GNP has a coordinate system $\{\mathbf{C}_j; \mathbf{U}_j, \mathbf{V}_j, \mathbf{W}_j\}$ for $j = 1, 2$, with $\mathbf{C}_j$ as the origin, mutually perpendicular unit-length vectors create a right-handed orthonormal $\mathbf{W}_j = \mathbf{U}_j \times \mathbf{V}_j$. Points on the mid-surface of an elliptical GNP can be represented as appeared in Eq. (3) [42].

$$\mathbf{X}_j = \mathbf{C}_j + s_j \mathbf{U}_j + t_j \mathbf{V}_j \quad (3)$$

Knowing the semi-minor and semi-major axis lengths of the GNP helps constraining the parameters (s_j, t_j) as depicted in Eq. (4).

$$\left(\frac{s_j}{a_j}\right)^2 + \left(\frac{t_j}{b_j}\right)^2 \leq 1 \quad (4)$$

Here a_j and b_j as the semi-major and semi-minor lengths. Eq. (4) helps to restrain the elliptical GNPs' limits in the appropriate range. Fig. 1**(a)** exhibits schematics of graphene nanoplatelets with their semi-minor and semi-major lengths and mid-surface vectors. Fig. 1**(b)** shows a CNT with length l_i, starting and ending points. The rectilinear CNT near a GNP can be assumed reasonably due to linear dependence when CNTs are in contact with each other, which means although the physical character of the CNTs is branched, their high aspect ratio denotes that any effects of CNT curvature are generally at a distance, and assumption of rectilinear CNTs should be sufficient.

In this study, the prediction of the electrical resistivity is carried out using a 3D RVE with a random distribution of CNTs and GNPs. Fig. 2 shows a schematic representation of CNTs and GNPs with random orientations and different volume fractions in the RVE. The CNTs are impenetrable and separated from each other with different separation distances. Obviously GNPs are randomly distributed between CNTs in both low and high volume fraction RVEs. Scattered CNTs spread the GNPs' surfaces for higher volume fraction RVE. In the model, any direct contact or overlapping between the dispersed nanofillers is prohibited and the shortest distance between two nanofillers must be larger than the van der Waals' distance, 0.34 nm. To this end, the shortest distances between a newly added CNT and the existing CNTs are calculated and

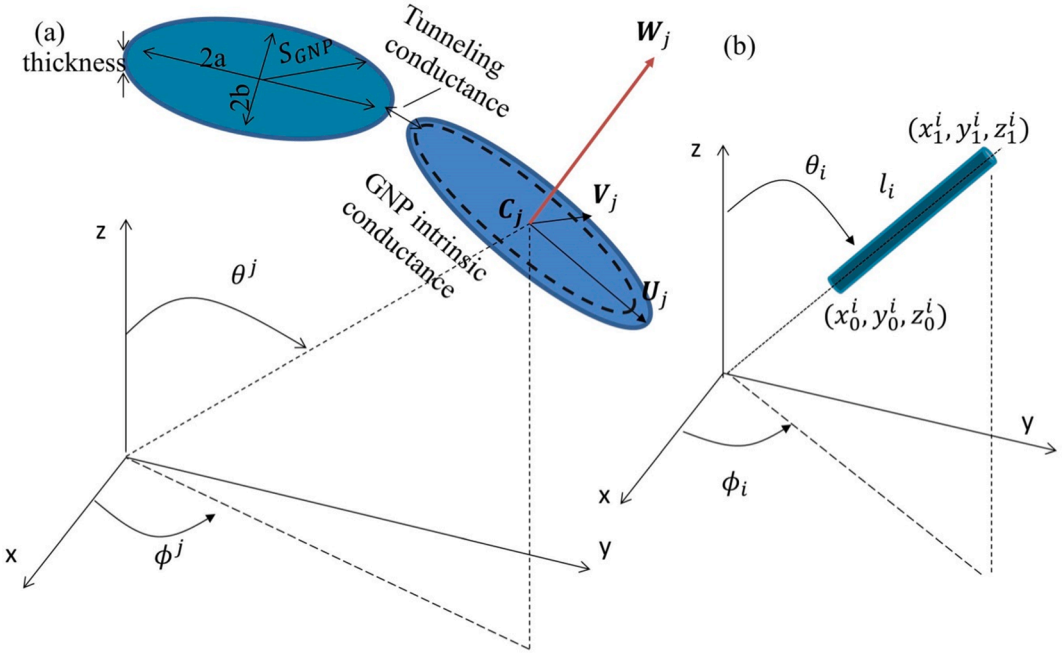

Fig. 1. Schematics of (a) graphene nanoplatelets having both intrinsic and tunneling resistances (b) CNT having a specific position, polar and azimuthal angles. (For interpretation of the references to colour in this figure legend, the reader is referred to the web version of this article.)

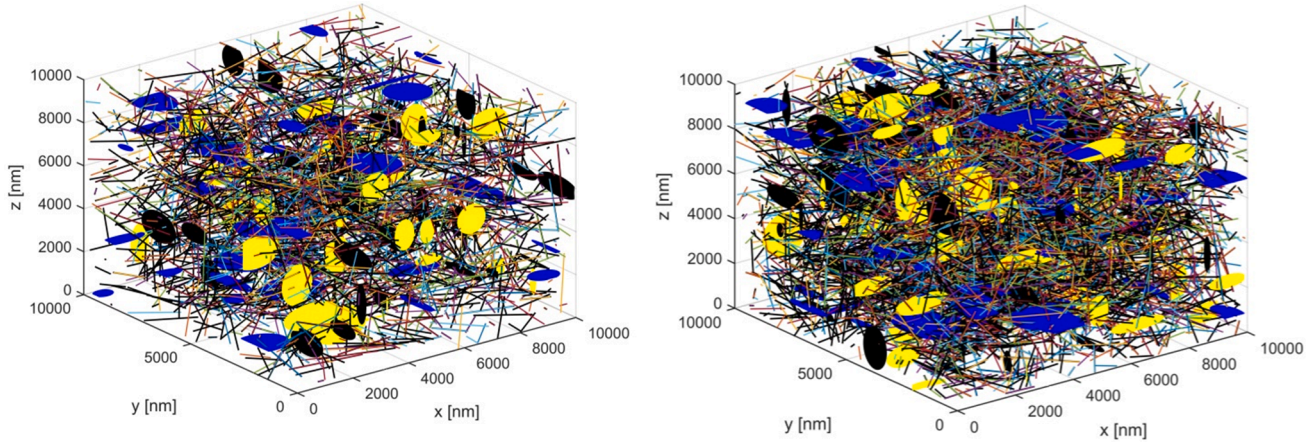

Fig. 2. Diagrams of 3% and 6% CNT/GNP polymer nanocomposites including randomly oriented nanofillers. (For interpretation of the references to colour in this figure legend, the reader is referred to the web version of this article.)

only nanofillers that passed the previous condition are kept in the RVE. Also, newly generated GNPs are retained if they do not penetrate with other produced nanofillers and has to be discarded once penetrating with the existing fillers. As a result, the RVE with a fixed volume ratio of two nanofillers can be established. The CNT orientation is uniform and independent of the coordinate system. The simulations were carried out by progressively adding nanofillers inside the volume and examining the required volume fraction. The algorithm would not stop until the required fillers are randomly assigned inside the cuboid. The RVE dimensions are set as 10 μm. The diameter and length of the CNTs are set as 20 nm and 0.1–3 μm, respectively.

2.2. Electrical resistance

The electrical resistance of CNT/polymer nanocomposites depends heavily on the CNT network. Prior to identifying the overlap and contact status among CNTs and GNPs in the network, the intrinsic resistance of each filler is calculated. Along a CNT between two nearest contact points j and k happens intrinsic electrical resistance as calculated by Eq. (5).

$$R_{jk} = \frac{4(1+\alpha_{\mathrm{CNT}}\Delta T)l_{jk}}{\sigma_{\mathrm{CNT}}\pi d^2} \tag{5}$$

Here l_{jk} is the length between the contact points j and k. Symbols d, α_{CNT} and σ_{CNT} are the CNT's diameter, TCR and intrinsic electrical conductivity, respectively.

For an elliptical GNPs with major length $2a_0$ and minor length $2b_0$, the electrical resistance is defined as depicted in Eq. (6).

$$R_{\mathrm{GNP}} = \frac{4a_0R_s(1+\alpha_{\mathrm{GNP}}\Delta T)}{\pi b_0} \tag{6}$$

Here R_s is the sheet resistance of graphene.

Tunneling resistance is represented by the quantum resistance between two neighboring fillers at the appropriate separation distance. The tunneling effects cannot be ignored in the polymer thickness between two nanofillers surfaces is smaller than the cutoff distance $d_{\mathrm{cutoff}} = 2\mathrm{nm}$. Prior to evaluating the contact among fillers, the current–voltage relationship formula is derived first by adopting Landauer-Buttiker formula as appeared in Eq. (7) [43].

$$I = \frac{2e}{h}\int_0^{\infty}\tau M\left[\frac{1}{e^{\frac{E-\mu-eV}{k_BT}}+1} - \frac{1}{e^{\frac{E-\mu}{k_BT}}+1}\right]\mathrm{d}E \tag{7}$$

Here M is the total number of conduction channels and τ is the transmission probability for electrons to tunnel through the polymer barrier. The transmission probability is approximated by Eq. (8).

$$\tau = \begin{cases} \exp(-\dfrac{d_{\mathrm{vdW}}}{d_{\mathrm{tun}}}) 0 < d_{mn} \le d_{\mathrm{vdW}} \\ \exp\left(-\dfrac{d_{mn}-d}{d_{\mathrm{tun}}}\right) d_{\mathrm{vdW}} < d_{mn} \le d_{\mathrm{cutoff}} \end{cases} \tag{8}$$

Here $d_{\mathrm{tun}} = \frac{\hbar}{\sqrt{8m_e\Delta E}}$ is the tunneling distance [44]. In addition, the minimum distance that separates two nanotubes is never smaller than the van der Waals (vdW) distance to insure no force between CNTs [45]. The electrical resistance can be estimated as the tunneling resistances of connected pairs of CNTs.

The above equation can be approximated by the first-order Taylor expansion of the term τM as depicted in Eq. (9) [46].

$$I = \frac{2e}{h}\left\{\int_{\mu}^{\mu+eV}\tau M\mathrm{d}E + \frac{\pi^2}{6}(k_BT)^2 \times \frac{d[\tau M]}{d\mathrm{E}}\Big|_{\mu}^{\mu+eV} + O\left(\frac{k_BT}{\mu}\right)^4\right\} \tag{9}$$

Other approximations could be made as written in Eq. (10).

$$\int_{\mu}^{\mu+eV}\tau M\mathrm{d}E \approx eVM\tau$$

$$\frac{d[\tau M]}{dE}\Big|_{\mu}^{\mu+eV} \approx eVM\frac{d^2\tau}{dE^2}\Big|\mu \tag{10}$$

The mode of conduction by jumps of electrons through energy barriers at intersections is named quantum tunneling. Electrical resistance can be deduced by an averaged 1D tunneling model. The tunneling resistance is calculated by Eq. (11).

$$R^{\mathrm{tun}} = \frac{V}{I} = \frac{h}{2e^2}\cdot\frac{1}{M\tau\left\{1+\frac{\pi^2}{6}\left(\frac{k_BT}{\Delta E}\right)^2\ln\tau(\ln\tau+1)\right\}} \tag{11}$$

Here $\frac{h}{2e^2} = 12.9054\mathrm{k}\Omega$ is quantum resistance and ΔE is the height of barrier potential which is the difference of the work functions between the nanofiller and the polymer.

If the shortest distance between two nanofillers is less than the cutoff distance, the two nanofillers are considered to be in electrical contact. The shortest distance between the axes of two CNTs is presented by Eq. (12) [47].

$$d_{ij} = \frac{\|v_{ij}(v_i \times v_j)\|}{\|v_i \times v_j\|} \tag{12}$$

Here v_i and v_j are the direction vectors along the i th and j th CNTs, which are connected by the vector v_{ij}.

$$v_{\xi} = \left(x_{\xi}^1 - x_{\xi}^0, y_{\xi}^1 - y_{\xi}^0, z_{\xi}^1 - z_{\xi}^0\right), \xi = i,j \tag{13}$$

$$v_{ij} = (x_i^0 - x_j^0, y_i^0 - y_j^0, z_i^0 - z_j^0) \tag{14}$$

Returning to two individual GNPs with $\{s_0, t_0\}$ and $\{s_1, t_1\}$ as multipliers for **U** and **V** vectors; suppose that $\mathbf{p} = [s_0 \quad t_0 \quad s_1 \quad t_1]^T$, $\mathbf{k}_j = [0 \quad 0 \quad 0 \quad 0]^T$, $d_j = 1/2$, for $j = 1, 2$. To ease computation scheme, $\boldsymbol{H}_0$ and $\boldsymbol{H}_1$ are used as matrices including semi-minor and semi-major lengths of two GNPs [42].

$$\boldsymbol{H}_0 = \begin{bmatrix} 1/a_0^2 & 0 & 0 & 0 \\ 0 & 1/b_0^2 & 0 & 0 \\ 0 & 0 & 0 & 0 \\ 0 & 0 & 0 & 0 \end{bmatrix}, \boldsymbol{H}_1 = \begin{bmatrix} 0 & 0 & 0 & 0 \\ 0 & 0 & 0 & 0 \\ 0 & 0 & 1/a_1^2 & 0 \\ 0 & 0 & 0 & 1/b_1^2 \end{bmatrix} \tag{15}$$

Writing an equivalent equation for restraining s_j and t_j in the ellipse could help the computation scheme [48].

$$\frac{1}{2}\mathbf{P}^T\boldsymbol{H}_j\mathbf{P} + \mathbf{k}_j^T\mathbf{P} + d_j \le 0 \tag{16}$$

The distance between two GNPs is known as the shortest distance between two elliptical disks in the space which is defined as [49].

$$\varnothing(s_0, t_0, s_1, t_1) = \frac{1}{2}\|\mathbf{X}_0(s_0, t_0) - \mathbf{X}_1(s_1, t_1)\|^2 = \frac{1}{2}\mathbf{p}^T\boldsymbol{Q}\mathbf{p} + \mathbf{f}^T\mathbf{p} + \frac{1}{2}\|\Delta\|^2 \tag{17}$$

Where $\mathbf{p} = [s_0 t_0 s_1 t_1]^T$, tensor $\boldsymbol{Q}$ and vectors Δ and $\mathbf{f}$ are indicated in Eq. (18).

$$\boldsymbol{Q} = \begin{bmatrix} 1 & 0 & -\mathbf{U}_0^T.\mathbf{U}_1 & -\mathbf{U}_0^T.\mathbf{V}_1 \\ 0 & 1 & -\mathbf{V}_0^T.\mathbf{U}_1 & -\mathbf{V}_0^T.\mathbf{V}_1 \\ -\mathbf{U}_0^T.\mathbf{U}_1 & -\mathbf{V}_0^T.\boldsymbol{U}_1 & 1 & 0 \\ -\mathbf{U}_0^T.\mathbf{V}_1 & -\mathbf{V}_0^T.\mathbf{V}_1 & 0 & 1 \end{bmatrix}, \Delta = \mathbf{C}_0 - \mathbf{C}_1, \mathbf{f}$$
$$= \begin{bmatrix} \mathbf{U}_0^T.\Delta \\ \mathbf{V}_0^T.\Delta \\ -\mathbf{U}_1^T.\Delta \\ -\mathbf{V}_1^T.\Delta \end{bmatrix} \tag{18}$$

The wrinkle of GNP is ignored for the sake of simplicity. The shortest distances of each GNP are computed from the other GNPs using the "fmincon" function of MATLAB based on the initial value of (s_0, t_0, s_1, t_1). If the shortest distance is in the tunneling range, the two GNPs are in connection. The shortest distance between a CNT and GNP is evaluated by a similar procedure.

The intersection resistance includes intrinsic resistances and the tunneling resistances. CNTs or GNPs which are distanced in a range shorter than the cutoff distance are used to evaluate electrical resistivity. In the RVE, each path is recognized by a set of serial resistors in contact. Considering the total number of resistances in each conductive path leads to Eq. (19) [50].

$$R_p = N_{\mathrm{CNT}}R_{\mathrm{CNT}} + N_{\mathrm{GNP}}R_{\mathrm{GNP}} + \sum R_{\mathrm{tun}} \tag{19}$$

Here N_{CNT} and N_{GNP} are the number of nanotubes and nanoplatelets in the path, respectively. Then, the effective electrical resistance is equivalent resistance of these conductive pathways assumed to be in parallel as described by Eq. (20).

$$\frac{1}{R_e} = \sum \frac{1}{R_p} \tag{20}$$

The effective electrical resistivity $\rho = RA/L$ is derived where A is the cross-sectional area of RVE and L is the length of RVE [51].

2.3. Piezoresistivity

It is well reported that the electrical resistivity can be diminished by the formation of new percolating networks of interconnected CNTs. Connected nanofillers have also role in improving the mechanical and thermal properties of nanocomposites [52]. Relocation and reorientation of the CNTs in the nanocomposite under strain control the properties of nanocomposites [53]. Reformation of the CNTs after the transformation leads to new distances between CNTs [54]. Not-stretchable and incompressible CNTs are assumed to be line elements with a defined radius. Assuming that the polymer is volume conserved, the dimensions of the RVE are incremented regarding the magnitude of strain $\Delta\varepsilon$ as shown in Eq. (21) [55].

$$L_x^{'} = L_x(1 + \Delta\varepsilon + \alpha\Delta T), L_y^{'} = L_y\left(1 - \nu_{xy}\Delta\varepsilon + \alpha\Delta T\right), L_z^{'} = L_z(1 - \nu_{xy}\Delta\varepsilon + \alpha\Delta T) \tag{21}$$

Where the prime explains the new variable after strain, ν is the polymer's Poisson's ratio and α is coefficient of temperature expansion (CTE) of matrix. The strain-induced CNT displacement within a deformed RVE can be declared by the displacement of its center. The center coordinates of the i-th CNT are transformed to new locations as described in Eq. (22).

$$\widetilde{x}_i^{'} = x_c^i(1 + \Delta\varepsilon + \alpha\Delta T), \widetilde{y}_i^{'} = y_c^i\left(1 - \nu_{xy}\Delta\varepsilon + \alpha\Delta T\right), \widetilde{z}_i^{'} = z_c^i(1 - \nu_{xz}\Delta\varepsilon + \alpha\Delta T) \tag{22}$$

A rotation based transformation for CNT's two ends with respect to its center leads to new starting and ending points of the i-th CNT after the strain as expressed in Eq. (23) [47].

$$\left(\widetilde{x}_i^0, \widetilde{y}_i^0, \widetilde{z}_i^0\right) = \left(\widetilde{x}_i^{'}, \widetilde{y}_i^{'}, \widetilde{z}_i^{'}\right) - \left[\left(\widetilde{x}_i^{'}, \widetilde{y}_i^{'}, \widetilde{z}_i^{'}\right) - \left(\overline{x}_i^0, \overline{y}_i^0, \overline{z}_i^0\right)\right] \times \begin{pmatrix} l_i \\ \widetilde{\widetilde{l}}_i \end{pmatrix}$$

$$\left(\widetilde{x}_i^1, \widetilde{y}_i^1, \widetilde{z}_i^1\right) = \left(\widetilde{x}_i^{'}, \widetilde{y}_i^{'}, \widetilde{z}_i^{'}\right) + \left[\left(\overline{x}_i^1, \overline{y}_i^1, \overline{z}_i^1\right) - \left(\widetilde{x}_i^{'}, \widetilde{y}_i^{'}, \widetilde{z}_i^{'}\right)\right] \times \begin{pmatrix} l_i \\ \widetilde{\widetilde{l}}_i \end{pmatrix} \tag{23}$$

where

$$\left(\overline{x}_i^0, \overline{y}_i^0, \overline{z}_i^0\right) = \left(x_i^0 + x_i^0\Delta\varepsilon + x_i^0\alpha\Delta T, y_i^0 - y_i^0\nu\Delta\varepsilon + y_i^0\alpha\Delta T, z_i^0 - z_i^0\nu\Delta\varepsilon + z_i^0\alpha\Delta T\right)$$

$$\left(\overline{x}_i^1, \overline{y}_i^1, \overline{z}_i^1\right) = \left(x_i^1 + x_i^1\Delta\varepsilon + x_i^1\alpha\Delta T, y_i^1 - y_i^1\nu\Delta\varepsilon + y_i^1\alpha\Delta T, z_i^1 - z_i^1\nu\Delta\varepsilon + z_i^1\alpha\Delta T\right)$$

$$\widetilde{l}_i = \sqrt{(x_i^1 - x_i^0)^2(1 + \Delta\varepsilon + \alpha\Delta T)^2 + \left[(y_i^1 - y_i^0)^2 + (z_i^1 - z_i^0)^2\right](1 - \nu\Delta\varepsilon + \alpha\Delta T)^2} \tag{24}$$

Applied strain will change the positions of crossed CNT junctions caused by axial movement. As the new electrical conduction paths are emerged, new resistances are calculated.

The variation in the j th GNP's center point with tension in the x-direction is calculated by Eq. (25).

$$\overline{c}_x^j = c_x^j(1 + \Delta\varepsilon + \alpha\Delta T), \overline{c}_y^j = c_y^j(1 - \nu\Delta\varepsilon + \alpha\Delta T), \overline{c}_z^j = c_z^j(1 - \nu\Delta\varepsilon + \alpha\Delta T) \tag{25}$$

Each of GNPs' mid-surface vectors is updated with the strain, Poisson's ratio and temperature as depicted in Eq. (26) [49].

$$\overline{\mathbf{U}}_j = \begin{Bmatrix} u_x^j(1 + \Delta\varepsilon + \alpha\Delta T) \\ u_y^j(1 - \nu\Delta\varepsilon + \alpha\Delta T) \\ u_z^j(1 - \nu\Delta\varepsilon + \alpha\Delta T) \end{Bmatrix}$$

$$\overline{\mathbf{V}}_j = \begin{Bmatrix} v_x^j(1 + \Delta\varepsilon + \alpha\Delta T) \\ v_y^j(1 - \nu\Delta\varepsilon + \alpha\Delta T) \\ v_z^j(1 - \nu\Delta\varepsilon + \alpha\Delta T) \end{Bmatrix} \tag{26}$$

When matrix is stretched into new condition, nanofillers are rotated towards the loading direction and the average distance between nanofillers increases due to re-orientation. The deformation induces

increment in the area between two adjacent nanofillers which is dependent on strain. Fig. 3 shows the strained RVE under 4% strain in the x-direction. The volume fraction of RVE is very low to clearly represent the strained nanofillers which are in black. After the strain, the increase of the shortest distance between updated nanofillers due to re-orientation of nanofillers could be evaluated. Change of width and thickness of RVE would lead to the change of area.

2.4. Temperature dependence

Temperature coefficient of resistance is used to evaluate the resistance change with temperature. The resistance change rate of the nanocomposite is described by $\Delta R/R_0$ and the temperature coefficient of resistance (TCR) is defined in Eq. (27).

$$\mathrm{TCR}(\%) = \frac{\Delta R}{R_0.\Delta T}{}^{*}100 \tag{27}$$

2.5. Computation steps

To assist the understanding of the computation steps toward the evaluation of piezoresistivity, a flow chard is given. Fig. 4 shows the flow chart containing steps of studying the piezoresistivity of nanocomposite using Monte Carlo simulation paired with percolation model. In the simulation, the cylinder and disk models are used to simulate CNTs and GNPs, respectively. The slender cylinders and thin disks are generated randomly for a given dimension, volume fraction, and arbitrary rotation. A 3D cubic RVE which includes both slender cylinders and thin disks is simulated considering the van der Waals distance to avoid penetration. According to the generated RVE, the intersections between every two nanofillers are evaluated by calculating the shortest distance between them. The nanofillers need to be in cutoff distance range to form conductive network, this implies tunneling resistance which means two nanofillers are close enough to let electrons pass. After building the intersection matrix between nanofillers, the formed conductive networks which contain connected nanofillers with their intrinsic and tunneling resistances in a group are recognized. The total resistance of nanocomposite is calculated considering these series of groups containing connected nanofillers as parallel paths. After giving an incremental mechanical strain, deformed RVE and strain-induced nanofiller movement within a deformed RVE can be expressed by a combination of rigid body displacement and rotation transformation. A new nanofiller network can be formed re-calculating the distance and the possible interactions between nanofillers. Eventually, the resistance of the nanocomposite at a fixed strain level can be re-evaluated to calculate the piezoresistivity of the nanocomposite.

3. Results and discussion

In order to study resistance–temperature dependence of the CNT/GNP strain sensors, various properties are investigated. The intrinsic electrical conductivity of CNTs is taken as $10^6 \mathrm{S/m}$ and the potential barrier height was approximately 1 eV. Other materials' physical and intrinsic parameters are delivered in Table 1, depicting 0.3, 1 eV, and 10 nm as the default Poisson's ratio of polymer, height of barrier potential, and diameter of CNTs, respectively.

Piezoresistive response is the centered subject in the area of sensor applications subjected to uniaxial tension. The procedure described in the formulation section is used to determine the piezoresistive response of nanocomposites. These conductive nanocomposites as self-sensing materials can sense owing to their fast response to applied strain resulting from the changes in the conductive network. When tension is applied, the electrical network becomes disconnected and the resistivity is increased. The piezoresistive response revealed a smooth curve with very small non-linear effects. The analytical results are compared with those from experiments [59] considering the random orientations of CNTs and GNPs. Fig. 5 shows that experimental data and analytical results are in good agreement for piezoresistivity of CNT/GNP polymer nanocomposites. Normalized resistance change varies linearly with increasing strain as a result of gradual break up of conductive paths. It is clearly shown that the piezoresistivity of nanocomposite decreases with more filler volume fraction. This is attributed to the increase in the number of junctions due to modification of conductive paths and entanglement of loosely packed networks. It is seen that nanocomposite-based strain sensors shows different linear and non-linear responses for different nanofillers. The non-linear piezoresistive response can be mainly attributed to the disruption of the conducting nanofiller network and tunneling effect between neighboring nanofillers. When strain sensor with sparse conductive network microstructures undergoes change from continuous morphology to discontinuous morphology upon stretching, strain sensors respond to the mechanical property with a non-linearity. Also, the increase of inter-distances between CNTs which are in contact with each other in very large numbers is the reason for linear sensitivity dependence on strain.

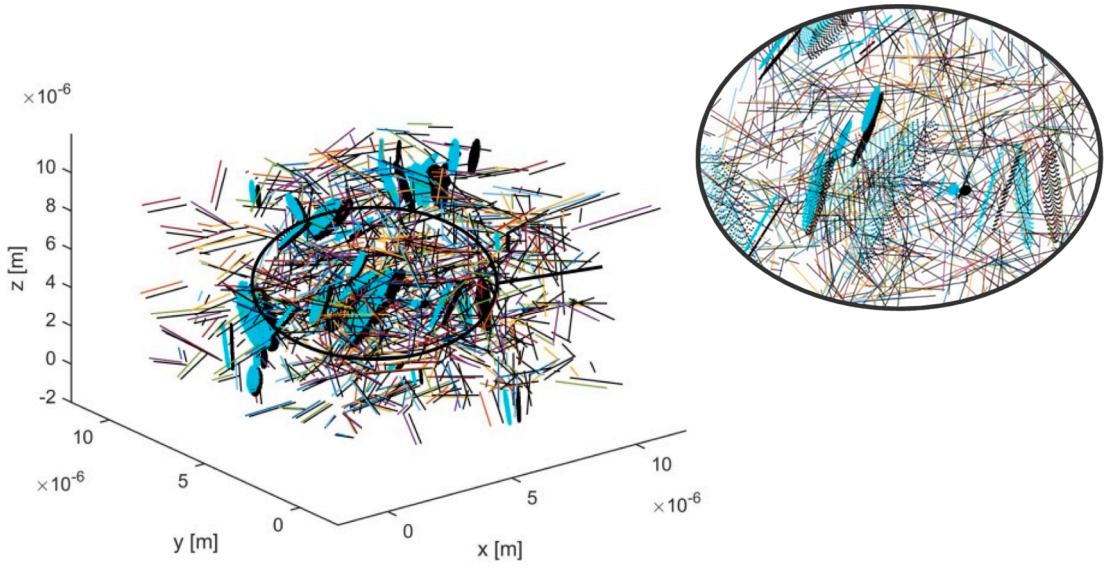

Fig. 3. Strained nanocomposite under 4% strain in the x-direction, the nanofillers in black are strained ones. (For interpretation of the references to colour in this figure legend, the reader is referred to the web version of this article.)

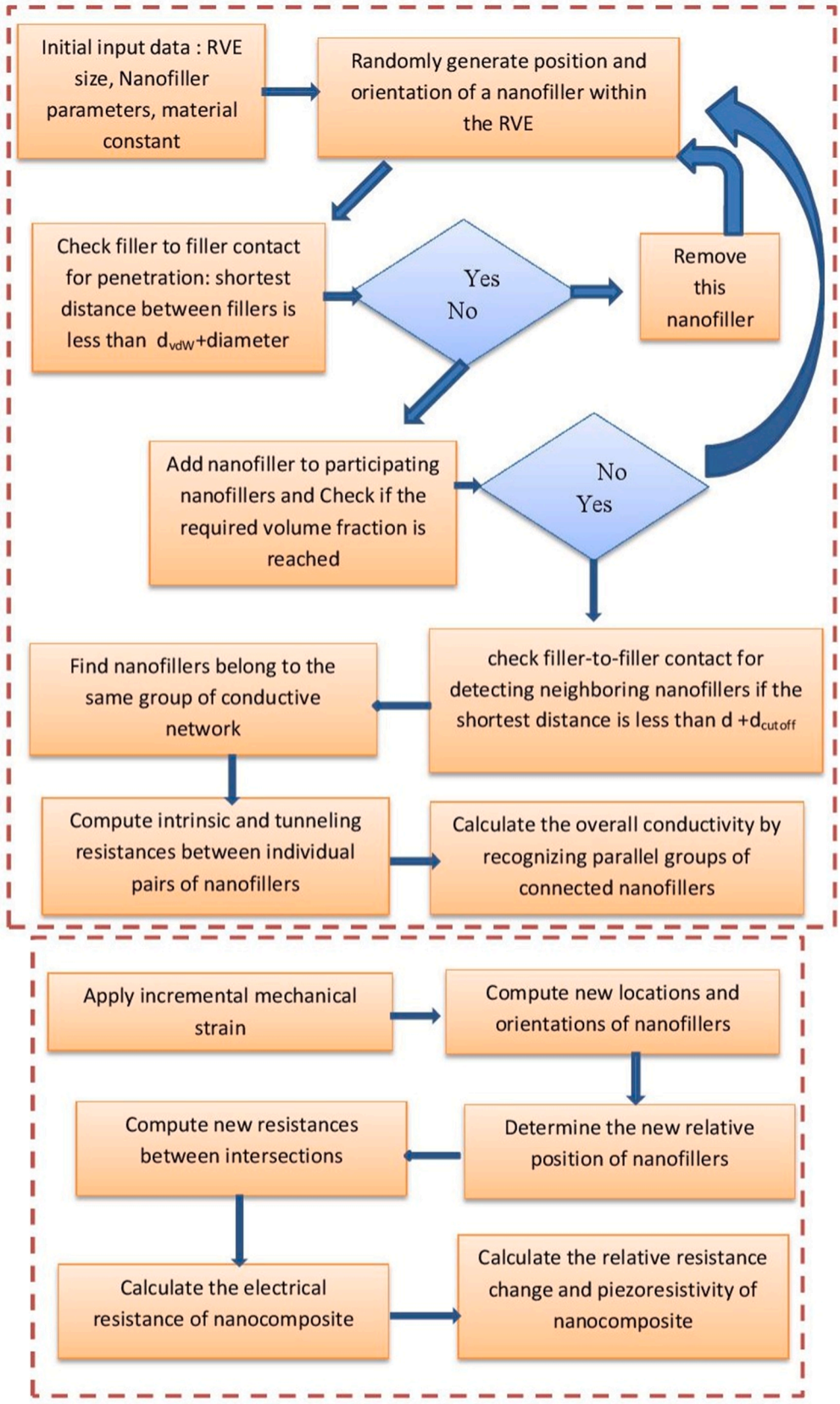

Fig. 4. Flow chart of different steps of Monte Carlo simulation approach toward the evaluation of piezoresistivity. (For interpretation of the references to colour in this figure legend, the reader is referred to the web version of this article.)

Table 1
Physical and intrinsic properties of polymer, CNT and GNP [15,56–58].

Material	Parameters	Value (unit)
Polymer	Poisson's ratio	0.15, 0.3, 0.45
	Height of barrier potential	0.5, 1, 2 eV
MWCNT	Diameter	5, 10, 20 nm
	Length	<3 μm
	Cutoff distance	2 nm
	Intrinsic conductivity	10,000 S/cm
	TCR	−0.0002 /K
	Work function	4.7 eV
GNP	Sheet resistance	280 Ω
	Semi-major axis	1 μm
	Semi-minor axis	0.5 μm
	Average radial size	1 μm
	Thickness	6 nm
	TCR	−0.00045
	Work function	4.7 eV
	Intrinsic resistivity	5e-5 Ω.cm

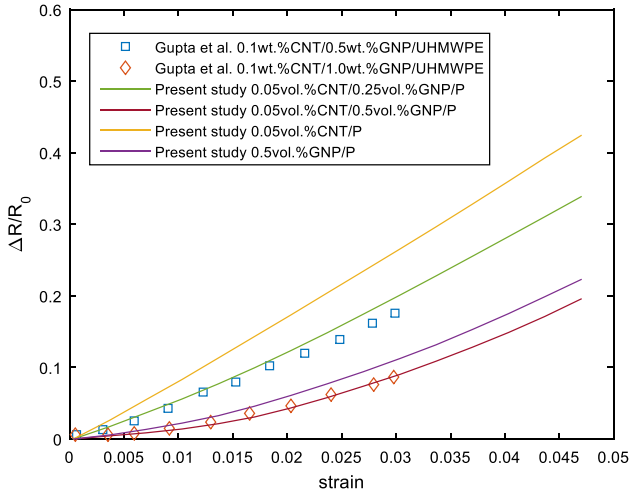

Fig. 5. Piezoresistivity of CNT/GNP polymer nanocomposites; comparison between experimental data and analytical results. (For interpretation of the references to colour in this figure legend, the reader is referred to the web version of this article.)

The relative resistance change $\Delta R/R_0$, where R_0 is the initial resistance before stretching for strain below 5% is plotted as a function of strain in Fig. 6. Comparing piezoresistivity for different polymer's Poisson's ratio in Fig. 6**(a)** reveals that with higher Poisson's ratio, in order to have the same resistance change rate, the extension should be greater. The destruction and formation of conductive networks, at the same time reduces the intensity of the piezoresistive response. Nanocomposites with high Poisson's ratio can adapt to the strain by changing the orientation of nanofillers due to the lateral contraction effect caused by Poisson's ratio. For this, it is assumed that the nanofiller and matrix strains are equal in the center of nanofiller parallel to the loading axis direction under small strain. However, it is noteworthy to mention that neglecting the CNT load bearing could overestimate the deformation state of the RVE. The piezoresistivity is calculated for different heights of barrier potentials as displayed in Fig. 6**(b)**. In a strain sensor, large barrier of the non-conductive materials may lead to the loss of electron transportation and would decrease conductivity. The well connected network with traversed connected paths results into diminished resistance. Fig. 6**(b)** shows that the piezoresistivity is lower for diminished height of barrier potential because the resistance is reduced due to the effect of cross overlapped CNTs' tunneling. Overlap phenomenon will be generated among the CNTs especially in the case of dense CNTs with more conductive channels and the matrix expansion affects the number of the overlaps between fillers. High potential barrier makes the transport of electrons difficult and thus a drastic change in electrical properties is produced. This severe influence by higher barrier potential on the piezoresistive sensitivity is related to opposition of matrix against electron transport.

Fig. 7 shows the influence of CNT diameter on the piezoresistivity of 1% CNT nanocomposite. By assuming default values for Poisson's ratio, height of barrier potential and intrinsic conductivity as given in Table 1, variation of CNT diameter leads to different piezoresistive sensitivities. Fillers possess high aspect ratio in the nanocomposite allow to form conductive paths with more contact points. When the nanocomposite is subjected to external forces such as the expansion of matrix, the electrical conductive network starts to change. While CNTs exist in matrix as a rigid line with no adaptive ability and larger effective distance, network is destroyed by these external tensions [60]. Along with this, shorter CNTs render a high density of contact points. With no beneficial factors for formation of new conductive networks due to inflexible CNTs' shape, the resistance is increased related to the relatively sparsely distributed CNTs in the nanocomposite. As such, strain causes more changes in the network configuration with larger but shorter CNTs.

It is well declared that the percolation threshold of nanocomposite is

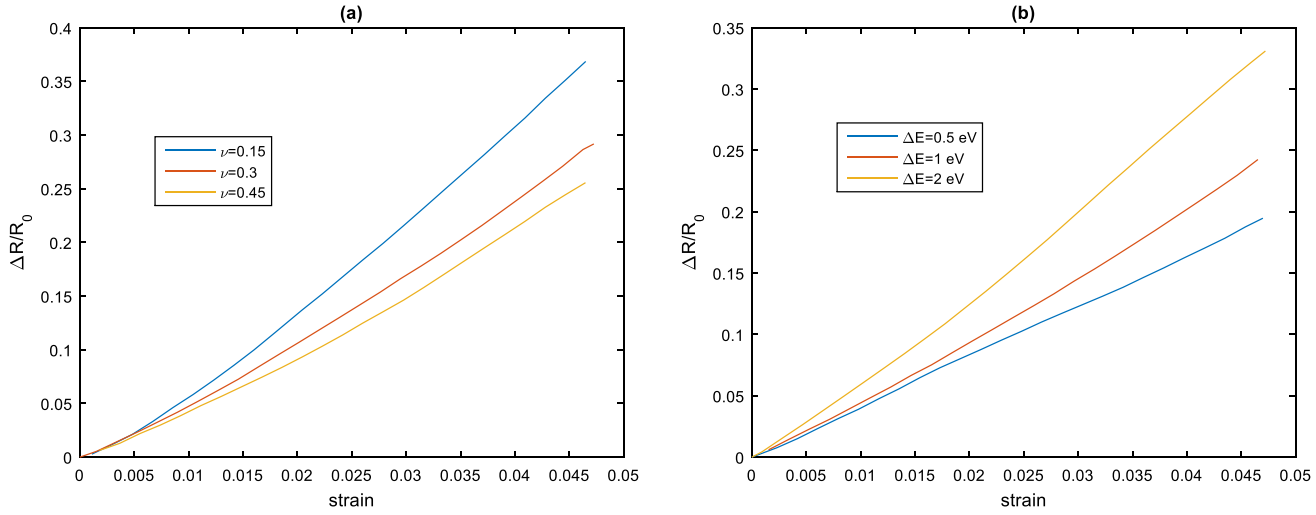

Fig. 6. Piezoresistivity of 0.5 vol% hybrid CNT/GNP polymer nanocomposites for different (a) polymer's Poisson's ratios and (b) heights of barrier potentials. (For interpretation of the references to colour in this figure legend, the reader is referred to the web version of this article.)

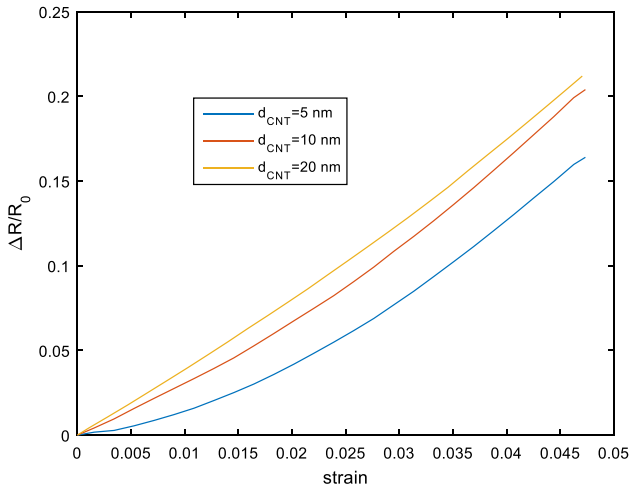

Fig. 7. Piezoresistivity of 1 vol% CNT polymer nanocomposite for different CNT diameters. (For interpretation of the references to colour in this figure legend, the reader is referred to the web version of this article.)

dominated by the filler selection with different shapes and geometries. CNTs could be separated by a distance known as separation gap which affects the transmission probability. As a result, the resistance increases due to the polymer layer between CNTs leaving a large part of the nanofillers not connected with each other. The addition of a small amount of fillers will cause a large scale overlap between them, where an electric conductive channel is effectively formed. Fig. 8 shows that selecting a suitable filler combination is an effective way to reduce the effect of separation gap and the network sparseness. Also, the geometry and distribution of fillers has a strong influence on the overall conductivity of the nanocomposite, in which high aspect ratio GNPs with their large surface area ease making connections with other nanofillers where synergism happens. Fig. 8 demonstrates that the physical properties of nanofillers affect the percolation threshold and resistivity of nanocomposite. It is worth noting that the percolation thresholds and conductivity values predicted by the model have a good agreement with experimental data [61]. It can also be seen that the CNT/P curve transition ends in lower resistivity than the GNP/P curve. This is because; CNTs overlap each other in a longer path than the GNPs to form conductive network.

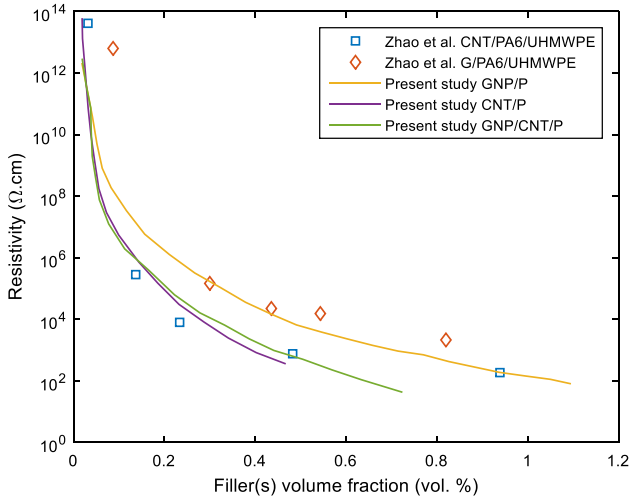

Fig. 8. Resistivity variation with filler(s) volume fraction for nanocomposites having different nanofillers, a comparison with experimental data [61]. (For interpretation of the references to colour in this figure legend, the reader is referred to the web version of this article.)

The reliability of the effective electrical conductivity of the nanocomposite by means of an analytical model is verified by comparison with the experimental data available as depicted in Fig. 9. To compare the theoretical model results with the experimental data for resistivity variation with MWCNT volume fraction, 10 nm and 2 μm were selected as MWCNT diameter and length and barrier height was selected as 1 eV. The applicability of the analytical model could be predicted over a selected range in which the ratio of removed CNTs due to overlap to accepted ones surges. This range contains volume fractions above percolation threshold (not-insulated material) and prior to converged values, which falls within the range of disregarded aggregation. Also, the assumed range of volume fraction seems reasonable because while mutual attraction between nanofillers from van der Waals forces could lead to aggregation [62], but there are physical limits on the aggregation formation even at higher values of volume fraction such as isolated CNTs dispersed in the matrix [63]. Also, CNT intrinsic electrical conductivity was changed from 300 S/cm to 500 S/cm, which showed a decrease in electrical resistivity. The theoretical prediction with default parameters leads to a good verification with Coelho and Morales experimental results [64]. The main reason for a different curve from Du et al. experimental data [65] is the randomness of CNTs in the theoretical model while Du et al. obtained nanocomposites with MWCNTs distributed along specific paths instead of uniform dispersion within the matrix.

The electrical resistivities predicted by the percolation model for different intrinsic resistivities of GNPs are presented as depicted in Fig. 10**(a)**. The values of the resistivity of the nanocomposite are higher with higher GNP intrinsic resistivities. The low intrinsic resistivity (ρ_{GNP}) resulted in a decrease in the opposition against electron jump at the region between GNPs. It is found that the results are consistent with the fact that percolation threshold decreases as the probability of electron transmission for the quantum tunneling increases. Fig. 10**(b)** shows the resistivity change with GNP volume fraction for different orientation states of GNPs. Considering the orientation state of GNPs in the polymer matrix, the electrical resistivity of nanocomposite increased apparently with higher alignment. This is due to the fact that, as the GNPs become aligned, fewer junctions and shorter lengths of percolation paths are available. In particular, filler alignment is a critical influential factor which destructs the percolation paths. Alignment causes bigger gap and fewer interactions which needs more energy for electron to tunnel through. Aligned GNPs can be bridged by misaligned GNPs reducing the resistivity considerably by introducing additional conduction pathways. The minimum filler distance is kept slightly low by randomly orientating the fillers at which the filler particle interconnection would be

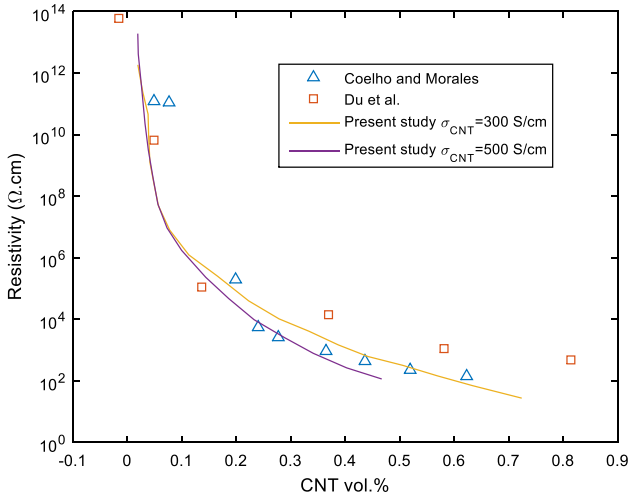

Fig. 9. Theoretical model versus experiments [64,65] for resistivity variation with CNT volume fraction. (For interpretation of the references to colour in this figure legend, the reader is referred to the web version of this article.)

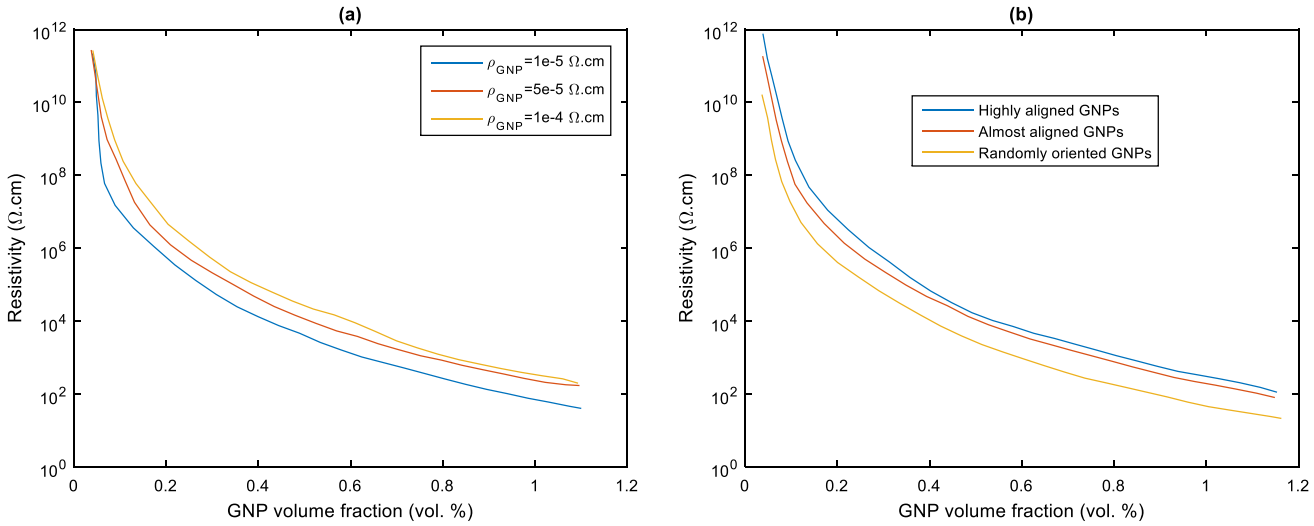

Fig. 10. Resistivity change with GNP volume fraction for different GNPs' (a) intrinsic resistivities and (b) orientation states. (For interpretation of the references to colour in this figure legend, the reader is referred to the web version of this article.)

maximized. Upon further enhancing the degree of orientation, more contact intersections come into being and enlarges the connective path lead to the growth of conductivity.

Fig. 11 illustrates the GNP semi-major axis length influence on the resistivity. GNPs act as bridges, increasing the number of conductive paths for electrical conduction. Fig. 11 shows that there is a direct relationship between the electrical resistivity and GNP semi-major length. A rapid decrease happens for a lower GNPs' semi-major length. This sharp decrease can be explained by the fact that the probability of an individual GNP to be a member of conductive network increases with their smaller size. This may be attributed to a larger number of smaller GNPs at a constant volume fraction helping the formation of networks for electron transmission.

Fig. 12 shows comparisons between analytical results and experimental data [61] of the temperature dependent resistivity for different CNT and GNP volume fractions. For more in-depth comparisons, nanocomposites having higher volume fraction of CNT and GNP are presented. Both NTC and PTC effects are apparent. The PTC effect shows that upon heating an electrically percolated nanocomposite, the number of conductive paths per unit volume within the polymer decreases. The decrease in resistivity with temperature (NTC) can be described by the

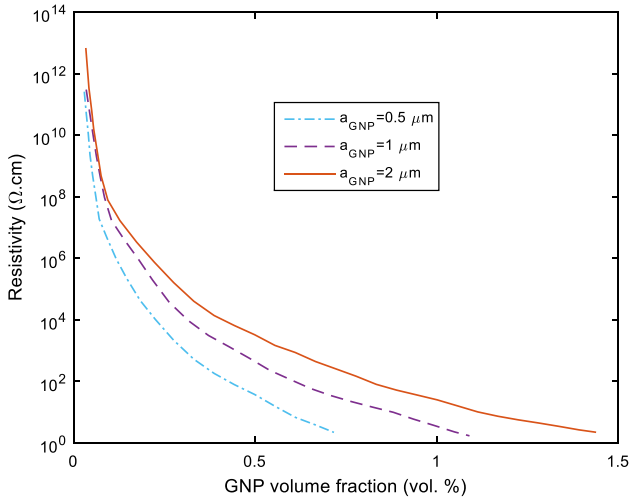

Fig. 11. Resistivity variation with GNP volume fraction for different GNPs' major-axis lengths. (For interpretation of the references to colour in this figure legend, the reader is referred to the web version of this article.)

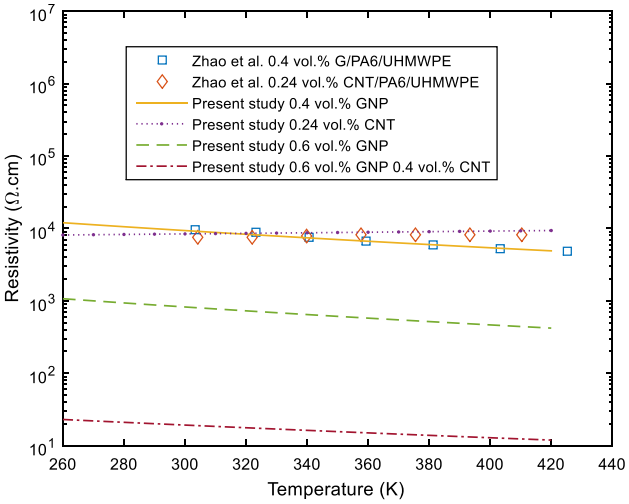

Fig. 12. Resistivity variation with temperature; comparisons between experimental data [61] and analytical results. (For interpretation of the references to colour in this figure legend, the reader is referred to the web version of this article.)

electron hopping activated at higher temperatures. The decrease in the dependence of the resistance on temperature is attributed to increased volume fraction which promotes the interaction between fillers and hinders the breakdown.

Fig. 13 shows the resistivity as a function of temperature with different CNT intrinsic electrical conductivities. The intrinsic conductivity of CNT is one of the parameters affecting electrical conduction in the insulating matrix due to manipulating free electrons transmission with high mobility along the CNTs. The temperature was increased up in steps of 10 °C. The results show that the NTC effect is dependent on the CNT intrinsic conductivity. At lower CNT intrinsic conductivity, the NTC effect becomes intensified. The reason is the lower temperature required to break off the junctions. It can also be seen that the resistivity is lower for higher CNT intrinsic conductivities which indicates that NTC is hampered because of the significant influence of interaction resistance between the CNTs.

Fig. 14 demonstrates the electrical resistivity as a function of temperature for different GNPs' sizes and intrinsic TCRs. It is seen from Fig. 14**(a)** that the electrical resistivity of the nanocomposite is affected

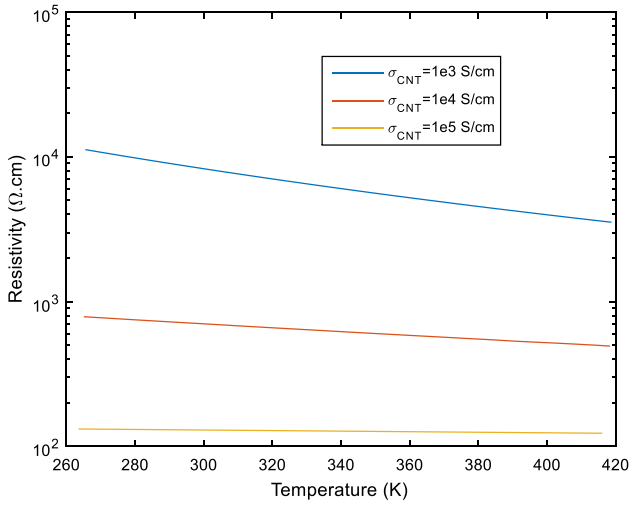

Fig. 13. Resistivity variation with temperature for 0.5 vol% CNT nanocomposite for different CNT intrinsic electrical conductivities. (For interpretation of the references to colour in this figure legend, the reader is referred to the web version of this article.)

by the microstructure size of the GNPs. Drop in resistivity with temperature is observed for smaller GNP's size. It may be expected that electrons are activated to hop over the non-conducting polymer matrix barrier at higher temperatures. At higher GNP size, the resistivity is less dependent to the temperature. A self-temperature-compensated behavior can be explained by a few conducting paths that are not affected by the temperature. The change of resistivity is plotted as a function of temperature for different GNPs' TCRs in Fig. 14**(b)**. Trends are consistent for all GNP TCRs to assess the thermoresistive sensitivity of the nanocomposite. The thermoresistive response confirms smaller change for lower GNPs' TCRs.

The relative resistance change as a function of temperature for different fillers' volume fractions is plotted in Fig. 15**(a)**. The results suggest that the fillers' volume fraction greatly affects the thermoresistive response of GNP/CNT polymer nanocomposite. The slopes of the curves represent TCR of the nanocomposite. The relative resistance change decreased with increased temperature for all fillers' volume fractions except one that reflects a prevalent negative TCR effect. On the other hand, the near zero TCR observed for 0.5 vol% GNP/CNT is due to the influencing of competing factors and the relative contribution of each one. For higher volume fraction, because of the restriction in thermal expansion imposed by fillers, the $\Delta R/R_0$ is negative. The high sensitivity for GNP nanocomposite suggests that competing mechanism of thermal expansion doesn't cancel the negative TCR of GNPs. The insignificant breakdown of interconnected GNP networks resulting from volumetric expansion is associated to the high structural stability of GNP network. For the low volume fraction, thermal expansion of the polymer matrix seems to dominate. The relative resistance change versus temperature for different CNT aspect ratios and volume fractions is presented in Fig. 15**(b)**. At higher volume fractions, the average separation distance reduces, increasing the effect of temperature rise. As noticed in Fig. 15**(b)**, the contribution of CNT aspect ratio dominates the relative resistance change with temperature, changing the number of junctions considerably. As seen in Fig. 15**(b)**, $\Delta R/R_0$ decreases with temperature and higher changes are observed for higher CNT aspect ratios. Finding negative TCR with higher sensitivities for CNTs with higher aspect ratios is attributed to electron jumping at a certain minimum gap (electron hopping activation) between longer paths. These results suggest that the evaluated changes of electrical resistance should have been higher if tunneling would have been the governing mechanisms rather than the volumetric expansion of the polymer matrix.

Fig. 16 presents the resistance change rate with temperature for different orientation states and volume fractions of CNTs. The relative contribution of each parameter depends on the initial condition, temperature range and changes in nanofillers network due to rotation and translation of nanofillers in the matrix. Results suggest that the change of relative resistance change with temperature differs significantly explained by different mechanism of breakdown of end-to-end aligned and side-to-length randomly oriented CNTs. The higher variation of thermoresistive response of randomly oriented CNTs indicates the dominant local rotational motions of CNTs over their translational movement. The possibility for the electrical resistance change is provided by the intrinsic thermoresistivity of the CNT and expansion of matrix. Sign change in the TCR for different almost aligned CNT volume fractions is due to more thermally-activated tunneling and variable range hopping.

4. Conclusions

The thermoresistive and piezoresistive responses of CNT/GNP/polymer nanocomposite were investigated using Monte-Carlo simulation method paired with percolation model. The analytical model considered the tunneling effect between fillers which played an

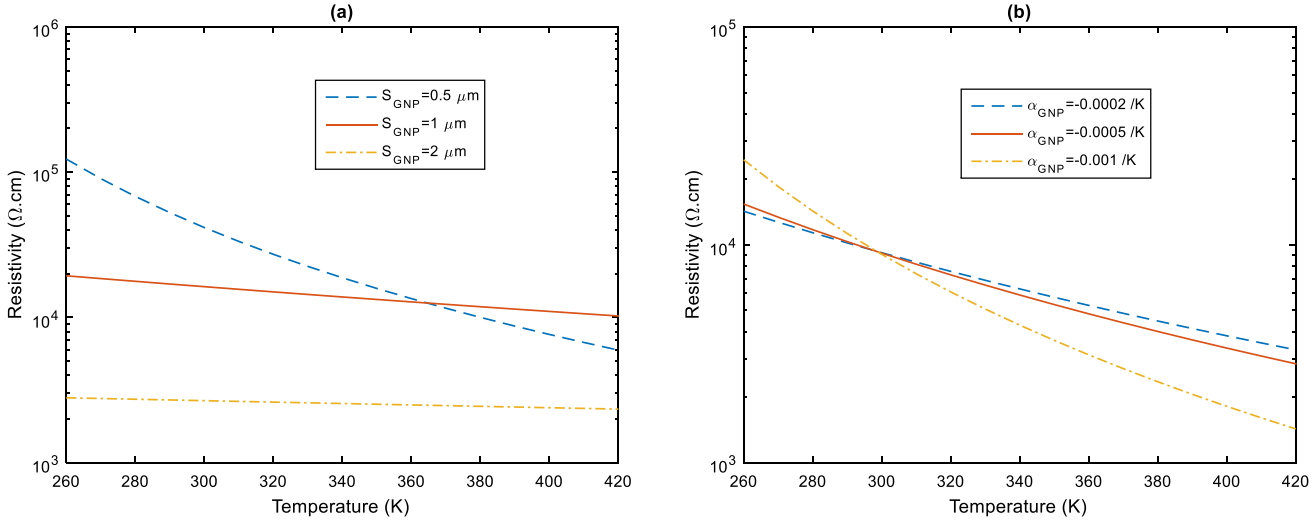

Fig. 14. Resistivity variation with temperature for different GNPs' (a) sizes and (b) intrinsic TCRs. (For interpretation of the references to colour in this figure legend, the reader is referred to the web version of this article.)

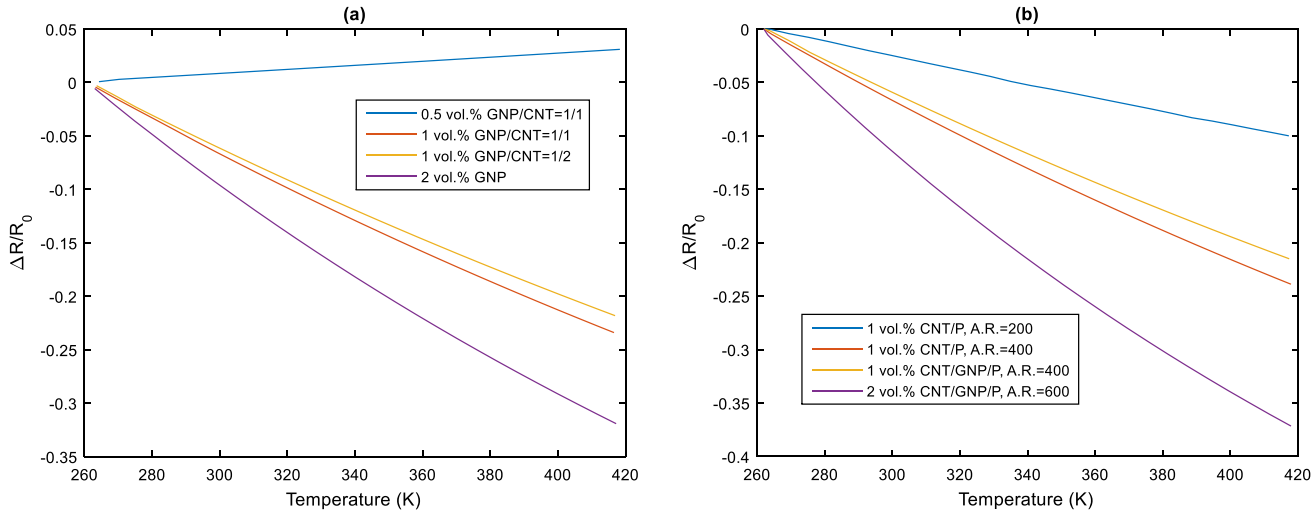

Fig. 15. Thermoresistivity of nanocomposites with different (a) nanofillers' volume fraction ratios and (b) CNTs' aspect ratios. (For interpretation of the references to colour in this figure legend, the reader is referred to the web version of this article.)

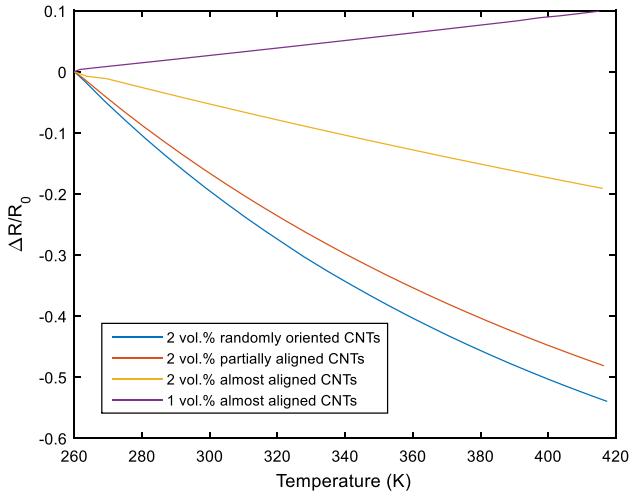

Fig. 16. Thermoresistivity of CNT polymer nanocomposite with different CNTs' orientation states. (For interpretation of the references to colour in this figure legend, the reader is referred to the web version of this article.)

important role in the results. The model predictions were in good agreement with the experimental data. The analytical investigations yielded insights into the underlying mechanisms that govern the thermoresistive response of GNP/CNT/polymer nanocomposite. Higher volume fractions of CNTs shifted the TCR to negative values attributed to intrinsic thermoresistive properties of CNTs. In addition to the size and aspect ratio of CNTs, their orientation states played an important role in thermoresistivity. With the increase of degree of orientation, the resistance began to decrease. It was found that smaller GNPs at relatively high volume fractions could decrease the electrical resistivity several orders. The results suggested that the mechanisms participating in the thermoresistive response are the thermal expansion and thermally activated electron hopping. The relative resistance change versus temperature calculated by the theory was dominated by thermal expansion at lower filler volume fractions.

CRediT authorship contribution statement

Mojtaba Haghgoo: Methodology, Software, Formal analysis, Writing – original draft. **Reza Ansari:** Validation, Resources, Writing – review & editing, Supervision, Investigation. **Sung-Hwan Jang:** Writing – review & editing, Investigation, Funding acquisition. **Mohammad Kazem Hassanzadeh-Aghdam:** Conceptualization, Data curation, Visualization. **Mohammad Nankali:** Conceptualization, Resources.

Declaration of Competing Interest

The authors declare that they have no known competing financial interests or personal relationships that could have appeared to influence the work reported in this paper.

Data availability

Data will be made available on request.

Acknowledgement

This work was supported by the National Research Foundation of Korea (NRF) grant funded by the Korea government (MSIT) (No.2020R1C1C1005273) and the research fund of Hanyang University (HY-2022-N).

References

[1] Oliva-Avilés A, et al. On the contribution of carbon nanotube deformation to piezoresistivity of carbon nanotube/polymer composites. Compos B Eng 2013;47:200–6.
[2] Zare Y. A model for tensile strength of polymer/clay nanocomposites assuming complete and incomplete interfacial adhesion between the polymer matrix and nanoparticles by the average normal stress in clay platelets. RSC Adv 2016;6(63):57969–76.
[3] Kundalwal SI, Rathi A. Improved mechanical and viscoelastic properties of CNT-composites fabricated using an innovative ultrasonic dual mixing technique. J Mech Behav Mater 2020;29(1):77–85.
[4] Zare Y, Rhee KY. A multistep methodology for calculation of the tensile modulus in polymer/carbon nanotube nanocomposites above the percolation threshold based on the modified rule of mixtures. RSC Adv 2018;8(54):30986–93.
[5] Zare Y. "a" interfacial parameter in Nicolais-Narkis model for yield strength of polymer particulate nanocomposites as a function of material and interphase properties. J Colloid Interface Sci 2016;470:245–9.
[6] Rathi A, Kundalwal SI. Mechanical and fracture behavior of MWCNT/ZrO2/epoxy nanocomposite systems: Experimental and numerical study. Polym Compos 2020;41(6):2491–507.
[7] Zare Y. Study on interfacial properties in polymer blend ternary nanocomposites: role of nanofiller content. Comput Mater Sci 2016;111:334–8.
[8] Fortunato, M., et al. Development and characterization of a piezoresistive polyurethane/GNP coating for strain sensing applications. in 2020 IEEE 20th International Conference on Nanotechnology (IEEE-NANO). 2020. IEEE.
[9] Lu S, et al. Highly sensitive graphene platelets and multi-walled carbon nanotube-based flexible strain sensor for monitoring human joint bending. Appl Phys A 2019;125(7):1–11.

[10] Jeong C, Park Y-B. Exfoliated graphite nanoplatelet-carbon nanotube hybrid composites for compression sensing. ACS Omega 2020;5(6):2630–9.
[11] Lee C, Jug L, Meng E. High strain biocompatible polydimethylsiloxane-based conductive graphene and multiwalled carbon nanotube nanocomposite strain sensors. Appl Phys Lett 2013;102(18):183511.
[12] Brigandi PJ, Cogen JM, Pearson RA. Electrically conductive multiphase polymer blend carbon-based composites. Polym Eng Sci 2014;54(1):1–16.
[13] Feng C, Jiang L. Investigation of uniaxial stretching effects on the electrical conductivity of cnt–polymer nanocomposites. J Phys D Appl Phys 2014;47(40):405103.
[14] Zare Y, Rhee KY. Significances of interphase conductivity and tunneling resistance on the conductivity of carbon nanotubes nanocomposites. Polym Compos 2020;41(2):748–56.
[15] Jouni M, et al. A representative and comprehensive review of the electrical and thermal properties of polymer composites with carbon nanotube and other nanoparticle fillers. Polym Int 2017;66(9):1237–51.
[16] Tamburrano A, et al. The piezoresistive effect in graphene-based polymeric composites. Nanotechnology 2013;24(46):465702.
[17] Tung T, et al. Enhancing the sensitivity of graphene/polyurethane nanocomposite flexible piezo-resistive pressure sensors with magnetite nano-spacers. Carbon 2016;108:450–60.
[18] Zare Y, Rhee KY. Dependence of Z parameter for tensile strength of multi-layered interphase in polymer nanocomposites to material and interphase properties. Nanoscale Res Lett 2017;12(1):1–7.
[19] Peng W, et al. Effect of "Z" factor for strength of interphase layers on the tensile strength of polymer nanocomposites. Polym Compos 2019;40(3):1117–22.
[20] Tanabi H, Erdal M. Effect of CNTs dispersion on electrical, mechanical and strain sensing properties of CNT/epoxy nanocomposites. Results Phys 2019;12:486–503.
[21] Ramalingame R, et al. Temperature Self-Compensated Strain Sensors based on MWCNT-Graphene Hybrid Nanocomposite. J Compos Sci 2019;3(4):96.
[22] Zare Y, Rhee KY. Evaluation of the tensile strength in carbon nanotube-reinforced nanocomposites using the expanded Takayanagi model. JOM 2019;71(11):3980–8.
[23] Chang E, et al. Percolation mechanism and effective conductivity of mechanically deformed 3-dimensional composite networks: Computational modeling and experimental verification. Compos B Eng 2021;207:108552.
[24] Cen-Puc M, Oliva-Avilés A, Avilés F. Thermoresistive mechanisms of carbon nanotube/polymer composites. Physica E 2018;95:41–50.
[25] Maffucci A, et al. Modeling, fabrication, and characterization of large carbon nanotube interconnects with negative temperature coefficient of the resistance. IEEE Trans Compon Packag Manuf Technol 2017;7(4):485–93.
[26] Morais MV, et al. On the effect of electric field application during the curing process on the electrical conductivity of single-walled carbon nanotubes–epoxy composites. Carbon 2019;150:153–67.
[27] Sibilia S, et al. Temperature-dependent electrical resistivity of macroscopic graphene nanoplatelet strips. Nanotechnology 2021;32(27):275701.
[28] Tran M, et al. 3D sprayed polyurethane functionalized graphene/carbon nanotubes hybrid architectures to enhance the piezo-resistive response of quantum resistive pressure sensors. Carbon 2020;168:564–79.
[29] Jang, S.-H. and Y.-L. Park, Carbon nanotube-reinforced smart composites for sensing freezing temperature and deicing by self-heating. Nanomaterials and Nanotechnology, 2018. **8**: p. 1847980418776473.
[30] Wu L, et al. Screen-printed flexible temperature sensor based on FG/CNT/PDMS composite with constant TCR. J Mater Sci Mater Electron 2019;30(10):9593–601.
[31] Lasater KL, Thostenson ET. In situ thermoresistive characterization of multifunctional composites of carbon nanotubes. Polymer 2012;53(23):5367–74.
[32] Li Q, et al. Carbon based polyimide nanocomposites thin film strain sensors fabricated by ink-jet printing method. Sens Actuators, A 2019;300:111664.
[33] Liu Y, et al. The effect of conductive network on positive temperature coefficient behaviour in conductive polymer composites. Compos A Appl Sci Manuf 2020;139:106074.
[34] Pech-Pisté R, et al. Multifunctional sensing properties of polymer nanocomposites based on hybrid carbon nanostructures. Mater Today Commun 2020;25:101472.
[35] Sanli A, et al. Piezoresistive performance characterization of strain sensitive multi-walled carbon nanotube-epoxy nanocomposites. Sens Actuators, A 2017;254:61–8.
[36] Turkani VS, et al. A carbon nanotube based NTC thermistor using additive print manufacturing processes. Sens Actuators, A 2018;279:1–9.
[37] Verma P, Schiffer A, Kumar S. Thermo-resistive and thermo-piezoresistive sensitivity of carbon nanostructure engineered thermoplastic composites processed via additive manufacturing. Polym Test 2021;93:106961.
[38] Razavi R, Zare Y, Rhee KY. A two-step model for the tunneling conductivity of polymer carbon nanotube nanocomposites assuming the conduction of interphase regions. RSC Adv 2017;7(79):50225–33.
[39] Razavi R, Zare Y, Rhee KY. A model for tensile strength of polymer/carbon nanotubes nanocomposites assuming the percolation of interphase regions. Colloids Surf A Physicochem Eng Asp 2018;538:148–54.
[40] Wang Z, Ye X. A numerical investigation on piezoresistive behaviour of carbon nanotube/polymer composites: mechanism and optimizing principle. Nanotechnology 2013;24(26):265704.
[41] Chen X, Alian A, Meguid S. Coupled electromechanical modeling of piezoresistive behavior of CNT-reinforced nanocomposites with varied morphology and concentration. Eur J Mech-A/Solids 2020;84:104053.
[42] Haghgoo M, Ansari R, Hassanzadeh-Aghdam M. Monte Carlo analytical-geometrical simulation of piezoresistivity and electrical conductivity of polymeric nanocomposites filled with hybrid carbon nanotubes/graphene nanoplatelets. Compos A Appl Sci Manuf 2022;152:106716.
[43] Bao W, et al. Tunneling resistance and its effect on the electrical conductivity of carbon nanotube nanocomposites. J Appl Phys 2012;111(9):093726.
[44] Namilae S, Li J, Chava S. Improved piezoresistivity and damage detection application of hybrid carbon nanotube sheet-graphite platelet nanocomposites. Mech Adv Mater Struct 2019;26(15):1333–41.
[45] Matos MA, Pinho ST, Tagarielli VL. Application of machine learning to predict the multiaxial strain-sensing response of CNT-polymer composites. Carbon 2019;146:265–75.
[46] Haghgoo M, Ansari R, Hassanzadeh-Aghdam M. Synergic effect of graphene nanoplatelets and carbon nanotubes on the electrical resistivity and percolation threshold of polymer hybrid nanocomposites. Eur Phys J Plus 2021;136(7):1–20.
[47] Haghgoo M, et al. A novel temperature-dependent percolation model for the electrical conductivity and piezoresistive sensitivity of carbon nanotube-filled nanocomposites. Acta Mater 2022;230:117870.
[48] Almohamad H, Selim SZ. An algorithm for computing the distance between two circular disks. App Math Model 2003;27(2):115–24.
[49] Haghgoo M, Ansari R, Hassanzadeh-Aghdam M. Prediction of piezoresistive sensitivity and percolation probability of synergetic CNT-GNP conductive network composite. Sens Actuators, A 2022;336:113414.
[50] Wichmann MH, et al. Piezoresistive response of epoxy composites with carbon nanoparticles under tensile load. Phys Rev B 2009;80(24):245437.
[51] Ventura IA, Zhou J, Lubineau G. Drastic modification of the piezoresistive behavior of polymer nanocomposites by using conductive polymer coatings. Compos Sci Technol 2015;117:342–50.
[52] Zare Y. Modeling the strength and thickness of the interphase in polymer nanocomposite reinforced with spherical nanoparticles by a coupling methodology. J Colloid Interface Sci 2016;465:342–6.
[53] Kumar S, Gupta TK, Varadarajan K. Strong, stretchable and ultrasensitive MWCNT/TPU nanocomposites for piezoresistive strain sensing. Compos B Eng 2019;177:107285.
[54] Spinelli G, et al. Experimental and theoretical study on piezoresistive properties of a structural resin reinforced with carbon nanotubes for strain sensing and damage monitoring. Compos B Eng 2018;145:90–9.
[55] Taya M, Kim W, Ono K. Piezoresistivity of a short fiber/elastomer matrix composite. Mech Mater 1998;28(1–4):53–9.
[56] Safdari M, Al-Haik MS. Synergistic electrical and thermal transport properties of hybrid polymeric nanocomposites based on carbon nanotubes and graphite nanoplatelets. Carbon 2013;64:111–21.
[57] Ebbesen T, et al. Electrical conductivity of individual carbon nanotubes. Nature 1996;382(6586):54–6.
[58] Khan T, et al. Insights to low electrical percolation thresholds of carbon-based polypropylene nanocomposites. Carbon 2021;176:602–31.
[59] Gupta TK, et al. Self-sensing and mechanical performance of CNT/GNP/UHMWPE biocompatible nanocomposites. J Mater Sci 2018;53(11):7939–52.
[60] Matos MA, et al. Predictions of the electro-mechanical response of conductive CNT-polymer composites. J Mech Phys Solids 2018;114:84–96.
[61] Zhao S, et al. Heating-induced negative temperature coefficient effect in conductive graphene/polymer ternary nanocomposites with a segregated and double-percolated structure. J Mater Chem C 2017;5(32):8233–42.
[62] Rathi A, et al. Adhesive and viscoelastic response of MWCNT/ZrO2 hybrid epoxy nanocomposites. J Mech Mater Struct 2021;16(3):281–92.
[63] Zare Y, Rhee KY. A simulation work for the influences of aggregation/agglomeration of clay layers on the tensile properties of nanocomposites. JOM 2019;71(11):3989–95.
[64] Coelho PH, Morales AR. Electrical conductivity, percolation threshold and dispersion properties of PMMA nanocomposites of hybrid conducting fillers. in 14th IEEE International Conference on Nanotechnology. IEEE; 2014.
[65] Du J, et al. Comparison of electrical properties between multi-walled carbon nanotube and graphene nanosheet/high density polyethylene composites with a segregated network structure. Carbon 2011;49(4):1094–100.